Accepted for publication in the AJ, April 25, 2007
Preprint typeset using LaTeX style emulateapj v. 11/12/01

STELLAR KINEMATICS IN THE REMOTE LEO II DWARF SPHEROIDAL GALAXY – ANOTHER BRICK IN THE WALL[1]

Andreas Koch[2,3], Jan T. Kleyna[4], Mark I. Wilkinson[5,6], Eva K. Grebel[2,7], Gerard F. Gilmore[5], N. Wyn Evans[5], Rosemary F. G. Wyse[8], Daniel R. Harbeck[9]
akoch@astro.ucla.edu

Accepted for publication in the AJ, April 25, 2007

ABSTRACT

We present the projected velocity dispersion profile for the remote (d=233 kpc) Galactic dwarf spheroidal (dSph) galaxy Leo II, based on 171 discrete stellar radial velocities that were obtained from medium-resolution spectroscopy using the FLAMES/GIRAFFE spectrograph at the European Southern Observatory, Chile. The dispersion profile of those stars with good membership probabilities is essentially flat with an amplitude of $6.6\pm0.7\,\mathrm{km\,s^{-1}}$ over the full radial extent of our data, which probe to the stellar boundary of this galaxy. We find no evidence of any significant apparent rotation or velocity asymmetry which suggests that tidal effects cannot be invoked to explain Leo II's properties. From basic mass modeling, employing Jeans' equation, we derive a mass out to the limiting radius of $(2.7\pm0.5)\times10^7\,M_\odot$ and a global mass to light ratio of 27–45 in solar units, depending on the adopted total luminosity. A cored halo profile and a mild amount of tangential velocity anisotropy is found to account well for Leo II's observed kinematics, although we cannot exclude the possibility of a cusped halo with radially varying velocity anisotropy. All in all, this galaxy exhibits dark matter properties which appear to be concordant with the other dSph satellites of the Milky Way, namely a halo mass profile which is consistent with a central core and a total mass which is similar to the common mass scale seen in other dSphs.

Subject headings: Galaxies: kinematics — Galaxies: dwarf — Galaxies: stellar content — Galaxies: structure — Galaxies: individual (Leo II) — Local Group

1. INTRODUCTION

In the two decades since the seminal work of Aaronson (1983) on the velocity dispersion of the Draco dwarf spheroidal galaxy (dSph), it has become observationally well-established that all of these lowest luminosity galaxies exhibit large overall velocity dispersions (of the order of $10\,\mathrm{km\,s^{-1}}$). Further, their radial velocity dispersion profiles are generally flat to very large radii (Kleyna et al. 2002, 2004; Koch et al. 2007a; Muñoz et al. 2006; Walker et al. 2006; though see Wilkinson et al. 2004 for the case of Draco and Ursa Minor). Coupled with their relatively large characteristic radii (of the order of hundreds of parsecs; see Fig. 1 in Gilmore et al. 2007) and low, star-cluster-like luminosities (Mateo 1998), these observations have led to the conclusion that these systems may be dominated by large amounts of dark matter on all spatial scales (see Mateo 1998; Gilmore et al. 2007 for recent reviews). Their estimated mass-to-light (M/L) ratios are often large, with values as high as several hundreds being reported in the literature[10]. The recent addition of eight new dSph candidates to the census of Milky Way satellites (Belokurov et al. 2006,2007; Irwin et al. 2007; Zucker et al. 2006a,b) has highlighted the bi-modal nature of the distribution of sizes for low-luminosity stellar systems. All known star clusters exhibit half-light radii smaller than 30pc while no dSph has a stellar core radius smaller than about 120pc (Belokurov et al. 2007; Gilmore et al. 2007). Given the apparent absence of dark matter in star clusters, this bi-modality adds circumstantial weight to the suggestion that dSphs are the smallest stellar systems to contain dynamically significant quantities of dark matter, making them particularly valuable for studies of its physical properties.

On the other hand, the above M/L estimates presuppose that the dSphs are in dynamical equilibrium, an assumption which is directly supported in, for example, the case of the Draco dSph by lack of any significant depth extent along our line of sight (e.g., Klessen et al. 2003). It has been argued, though, that the flat dispersion profiles and high apparent M/L ratios could be the results of tidal sculpting of these galaxies (e.g., Read et al. 2006a, 2006b, Westfall et al. 2006). While there are a few examples of close dSphs whose shape or kinematics appear to be affected by tides (e.g., Ursa Major II [Zucker et al. 2006];

[1] Based on observations collected at the European Southern Observatory at Paranal, Chile; proposal 171.B-0520(A), and on observations made through the Isaac Newton Groups' Wide Field Camera Survey Programme with the Isaac Newton Telescope operated on the island of La Palma by the Isaac Newton Group in the Spanish Observatorio del Roque de los Muchachos of the Instituto de Astrofisica de Canarias.

[2] Department of Physics and Astronomy, Astronomical Institute of the University of Basel, Binningen, Switzerland
[3] UCLA, Department of Physics and Astronomy, Los Angeles, CA, USA
[4] Institute for Astronomy, University of Hawaii, Honolulu, HI, USA
[5] Institute of Astronomy, Cambridge University, Cambridge, UK
[6] Department of Physics and Astronomy, University of Leicester, Leicester, UK
[7] Astronomisches Rechen-Institut, Zentrum für Astronomie Heidelberg, University of Heidelberg, Heidelberg, Germany
[8] The John Hopkins University, Baltimore, MD, USA
[9] Department of Astronomy, University of Wisconsin, Madison, WI, USA

[10] Throughout this paper, we will state all values of M/L in terms of V-band luminosity and solar units.

Ursa Minor [Palma et al. 2003]), the outer dSph satellites might be expected to be relatively unscathed by tidal perturbations. Galactic tides, if acting, would predominantly unsettle the outermost regions near the stellar boundary of these systems. Moreover, the Draco dSph, though being one of the close Galactic satellites, does not show any indication of structural perturbations (Odenkirchen et al. 2001; Segall et al. 2007). Coupled with the negligible ratio of ordered stellar rotational velocity (as a manifestation of tides; see Section 3 below) to the random motion in dSphs, the observations suggest that these galaxies are in fact the most dark matter dominated systems found to date. It is nevertheless valuable to compare the observed properties of dSphs with alternative models, and scenarios in which the dSphs are the remnants of tidally disrupted, dark-matter-free stellar systems have been investigated by a number of authors (e.g. Kroupa 1997; Kuhn & Miller 1989; Klessen & Zhao 2002).

Initially, information about the dSphs' dark matter content was mainly gleaned from estimates of their central velocity dispersion. Fortunately, in recent years wide field surveys have provided the opportunity to analyze stellar data covering the entire spatial extent of the dSphs and to investigate stellar kinematics even beyond their formal tidal limits as derived from King profile fits to their stellar density distributions (usually some tens of arc minutes; e.g., Odenkirchen et al. 2001; Kleyna et al. 2003, 2004; Tolstoy et al. 2004; Chapman et al. 2005; Mateo 2005; Muñoz et al. 2006; Walker et al. 2006; Wilkinson et al. 2006 and references therein; Koch et al. 2007a). Such studies are essential to reliably distinguish between the dark matter dominated and tidal disturbance scenarios.

The mass-density profiles of low-mass galaxies provide valuable information about the spatial distribution of dark matter on small scales. It has been suggested that halo density profiles, in particular the differentiation between cored and cusped halos, can provide an insight into the actual nature of cold dark matter (CDM; Read & Gilmore 2005; Colafrancesco et al. 2007; Gilmore et al. 2007). Numerical CDM simulations with high spatial resolution predict dark matter halos that exhibit a central density cusp, $\rho(r) \propto r^{-\alpha}$ with α=1–1.5 (e.g., Navarro, Frenk & White 1995; hereafter NFW; Diemand et al. 2005). By contrast, observations of the kinematics of massive galaxies are fully consistent with flat density cores (e.g., Gentile et al. 2004; Spekkens et al. 2005), which also appear to account for most of the available data for dSphs (Łokas 2002; Kleyna et al. 2003; Read & Gilmore 2005; Goerdt et al. 2006; Sánchez-Salcedo et al. 2006; Strigari et al. 2006; Wilkinson et al. 2006; Koch et al. 2007a, Wu 2007). The presence of central cores in the dark matter haloes of dSphs has important implications for the properties of dark matter as it may imply a maximum phase space density for dark matter which can be used to discriminate between competing dark matter candidates (CDM, Warm Dark Matter, self-interacting dark matter, etc.). One should bear in mind, however, that in the case of dSphs such inferences are subject to low-number statistics and uncertainties in the models and do not take account of the dynamical evolution of the dwarf galaxies' progenitor systems (Grebel et al. 2003).

In the light of all the above, the remote dSph Leo II provides an interesting test bench to investigate the dark matter content of Local Group dSphs. At its present-day Galactocentric distance of 233 kpc (Bellazzini et al. 2005) it is unlikely to have experienced severe Galactic tides unless it is on a very eccentric orbit that brings it close to the Milky Way. Previous kinematic data for this satellite were assembled in the study of Vogt et al. (1995; hereafter V95) for 31 stars within the core radius at 2.9′ (Irwin & Hatzidimitriou 1995). From these data, V95 found a M/L of 7 and concluded that Leo II must be embedded within a massive dark matter halo, although its dark matter properties are not extreme compared to those of other dSphs. On the other hand, Coleman et al. (2007), using photometry from the Sloan Digital Sky Survey, estimate a M/L of the order of 100, but predicate this value on the assumption that Leo II is purely dark matter dominated.

In this Paper, we shall investigate the dynamics of this particular galaxy by analyzing data for a large number of targets that reach out to the nominal outer optical radius at $\sim 9'$ (Irwin & Hatzidimitriou 1995; Coleman et al. 2007) thus enabling us to perform a full kinematical analysis of Leo II and to derive detailed information on its density distribution, its global M/L ratio and thus to answer the question of how well-behaved or extreme this galaxy is in terms of its dark matter content.

This paper is organized as follows: our data, their reduction and the derivation of individual velocities are described in §2. We investigate the extent of Leo II's apparent rotation in §3 and determine the galaxy's radial velocity dispersion profile in §4. These results allow us to derive mass and density profiles in §5, while §6 is dedicated to the question of whether Leo II's density profile shows a cusp or a core, as well as the importance of velocity anisotropy. Finally, we summarize our findings in §7.

2. OBSERVATIONS AND REDUCTION

In the framework of the ESO Large Programme 171.B-0520(A) (principal investigator: G. F. Gilmore), which aims at elucidating the kinematic and chemical characteristics of Galactic dSphs, five fields in Leo II were observed using the FLAMES multi-object facility at ESO's Very Large Telescope (Pasquini et al. 2002). Within the same programme, we also analysed the Carina dSph, which is described in detail in Koch et al. (2006). In a first paper concerning Leo II that made use of these data we presented this galaxy's spectroscopic metallicity and age distributions, which were derived using the near-infrared calcium triplet (CaT) calibration method (Koch et al. 2007b, hereafter Paper I). For details on our observing strategy, the data reduction and calibration techniques, we refer the reader to Paper I. In this section we briefly summarize the main steps taken.

2.1. *Target selection and acquisition*

The wide field of view of the FLAMES instrument, with a diameter of 25′, enables one to cover the whole projected area of the Leo II dSph with one single pointing, since its nominal tidal radius lies at 8.′7 (Irwin & Hatzidimitriou 1995). However, in order to achieve good sampling out to large radii and to yield more information about the stellar content near and beyond the tidal radius, we observed five

different (overlapping) fields in several instrument configurations, typically offset by 5′ with respect to each other (see Tables 1 and 2 in Paper I).

Our targets were drawn from photometry that was obtained by the Cambridge Astronomical Survey Unit[11] (CASU; Irwin & Lewis 2001) at the 2.5 m Isaac Newton Telescope (INT) on La Palma, Spain. From this data set we selected red giant candidates with magnitudes ranging from the tip of the red giant branch (RGB) at V∼18.5 mag down to 2.5 mag below the RGB tip, reaching as deep as 21 mag in apparent V-band magnitude. The total selected number of red giant candidates we could thus observe was 200. Their positions on the sky are depicted in Fig. 1.

The observations themselves were carried out using the identical strategy and instrumental setups as described in Paper I, i.e., we used the FLAMES instrument in combination with the GIRAFFE multifibre spectrograph in "low-resolution"-mode centered around the near-infrared CaT at 8550Å. This set up provides a full wavelength coverage of 8206–9400Å and a resolving power of $R \sim 6500$ per resolution element. Although we aimed at exposing each configuration for 6 hrs to reach a minimum nominal signal-to-noise (S/N) ratio of 20 pixel^{-1} at our spectral resolution of ~ 6500, the major part of the nights was hampered by bad sky conditions. Consequently, the median S/N achieved after processing the spectra is 12 pixel^{-1}, as defined from the variance in continuum bandpasses surrounding CaT region, from which we will determine our velocities in Sect. 2.3..

2.2. *Data reduction*

Details of the reduction process are given in Paper I. In summary, we used version 1.09 of the FLAMES data reduction system, girbldrs, and the associated pipeline version 1.05 (Blecha et al. 2000). After standard bias correction and flatfielding, the spectra were extracted by summing the pixels along a slit of width 1 pixel. The final rebinning to the linear wavelength regime was done using Th-Ar calibration spectra taken during the daytime.

Sky subtraction was facilitated by the allocation of about 20 fibers per configuration to blank sky. Because the pipeline did not perform reliable sky subtraction at the time the reduction was performed, custom reduction software was written to subtract sky background. First, the sky fibers were median-combined to produce an average sky for each field. Next, the sky was subtracted from each spectrum by modeling the observed spectrum as a second order polynomial plus the average sky, and minimizing the integral over wavelength of the absolute residual. The regions of the spectrum containing the lines of the CaT were excluded from the residual calculation because they are not expected to conform to our simple model of the spectrum. We estimate the accuracy of the final sky subtraction to be on the order of $\sim 3\%$, defined as the 1σ-dispersion of each sky-subtracted spectrum divided by the median of the sky spectrum.

Our data set was then completed by the co-addition of the dispersion-corrected and sky-subtracted science frames, weighted by the exposures' individual S/N, and subsequent rectification of the continuum.

2.3. *Radial velocities and Membership estimates*

In order to separate Leo II's RGB stars from Galactic foreground stars (Wyse et al. 2006), we determined the individual radial velocities of each target star by means of cross-correlation of the three calcium triplet lines against synthetic Gaussian template spectra using IRAF's[12] FXCOR task (see e.g., Kleyna et al. 2004). The templates were synthesized adopting representative equivalent widths of the CaT in red giants. The typical median velocity error achieved in this way is 2.4 km s^{-1}. Taking into account the possibility that the errors returned by FXCOR, which are based on the Tonry-Davis R-value (Tonry & Davis 1979), may in fact be under- or overestimated (e.g., Mateo et al. 1998; Kleyna et al. 2002), we pursued two different tests of our achieved accuracy. First, we determined a multiplicative constant to the formal velocity uncertainties by deriving radial velocities from the first two of the Ca lines at $\lambda\lambda$ 8498, 8452 Å and separately from the third line at 8662 Å. The constant was then obtained by requiring a reduced χ^2 of unity between these measurements. This procedure resulted in a re-scaling of the FXCOR velocity errors by a factor of 0.6. A second estimate of our velocity errors will be given in Sect. 2.4 by comparing our individual measurements to the published values from V95. A plot of velocity errors versus apparent magnitude and S/N is shown in Fig. 2.

Given Leo II's systemic velocity of ~ 76 km s^{-1} (V95), our velocity data set may contain a number of Galactic foreground stars along the galaxy's line of sight. However, owing to our selection of target stars whose colors and luminosities are consistent with their being members of Leo II's red giant branch and due to the much lower Galactic field star density, Leo II's velocity peak clearly stands out against the Galactic contribution (see Fig. 3; and Fig. 4 in Paper I). From the Besançon synthetic Galactic model (Robin et al. 2003) we would expect no more than 4 Galactic foreground stars within the our color-magnitude selection box and with velocities between 40 and 120 km s^{-1}, thus coinciding with Leo II's intrinsic population (see also Paper I).

An initial fit of a Gaussian velocity peak to the Leo II data yields a mean radial velocity and velocity dispersion of 78.7 km s^{-1} and 7.6 km s^{-1}. Our sample contains 23 apparent radial velocity non-members, which deviate by more than $5\,\sigma$ from this initial fit and thus were rejected from further analyses. The mean heliocentric velocity and line-of-sight velocity dispersion were finally determined via an iterative error-weighted maximum-likelihood fit assuming a Gaussian velocity distribution (e.g., Kleyna et al. 2002; Koch et al. 2007a). From this we find Leo II's mean radial velocity to be (79.1 ± 0.6) km s^{-1} with a global velocity dispersion of (6.6 ± 0.7) km s^{-1}. These values are in good agreement with the measurements of V95, who determined a mean velocity of (76.0 ± 1.3) km s^{-1} and a central velocity dispersion of (6.7 ± 1.1) km s^{-1} based on 31 high-resolution spectra of stars within the core radius at 2.′9 (Irwin & Hatzidimitriou 1995). If one adopts a conserva-

[11] see http://www.ast.cam.ac.uk/∼wfcsur

[12] IRAF is distributed by the National Optical Astronomy Observatories, which are operated by the Association of Universities for Research in Astronomy, Inc., under cooperative agreement with the National Science Foundation.

tive 2σ-cut in the velocity distribution in order to define membership of Leo II, 158 red giants are included in our sample. Relaxing the criterion to a $\pm 3\sigma$-cut yields 171 radial velocity member candidates. Given the low likelihood of interlopers in our sample, we will apply the 3σ-cut throughout the following analyses.

One noteworthy feature in the velocity histogram (Fig. 3, right panel) is the occurrence of an excess of stars at $\sim$85 km s^{-1}, whose velocities are approximately $0.9\,\sigma$ higher than the sample mean. This peak deviates by $1.8\,\sigma$ (taken as $\sqrt{N}$) from the best-fit curve. We note, however, that there is no apparent spatial correlation of the targets in this velocity range, nor is there any particular separation in color-magnitude space. In order to further investigate the possibility that we might be seeing an indication of a separate cold feature in our data, we ran an extensive number of Monte Carlo tests, where we generated normally distributed velocity samples centered on the observed mean velocity of Leo II assuming the previously derived dispersion, and which were additionally varied by the measurement errors. It turns out that $\sim$30% of the random data sets exhibit peaks in any one bin that deviate by as much as the observed $1.8\,\sigma$ so that the observed excess of stars is not significant above the $1\,\sigma$-level. Therefore we conclude that the potential second peak in Fig. 3 is most likely not a real velocity feature, but may rather be due to statistical fluctuations.

2.4. *Comparison with other data*

Out of the 31 stars observed by V95, 28 coincide with targets in our sample. Since their data are based on high-resolution spectroscopy obtained with the HIRES spectrograph at the Keck telescope, it is worthwhile to employ the stars in common between the two data sets to assess the quality and consistency of our own measurements. Fig. 4 shows a comparison of the radial velocities of these 28 stars as measured in this work to those from V95. An error-weighted linear least squares fit to these data yields the relation $v_{\rm V95} = (0.98 \pm 0.10)\, v_{\rm This\ work} + (0.5 \pm 7.6)$ with a r.m.s. scatter of 4.5 km s^{-1}. Although the latter value yields an estimate of the expected uncertainty in the velocities, it is clear that the errors of both studies and the individual S/N ratios have to be considered before one employs a simple re-scaling of our values to match the quoted r.m.s.[13]. Hence, we determined scale factors A in three bins of S/N (see right panel Fig. 4) such as to yield an agreement between our mean velocity errors and the scatter in terms of $\chi^2 = \sum \frac{(v_{\rm This\ work} - v_{\rm V95})^2}{A^2\,\sigma^2_{\rm This\ work} + \sigma^2_{\rm V95}}$, where the sum is over the stars in common. As a result, we rescaled our final errors by 1.46 (S/N$\leq$20), 1.31 (20 $\leq$S/N$\leq$ 40) and 1.18 (S/N$>$40). This leads to the uncertainties finally presented in Table 1.

Recently, Bosler et al. (2007) have performed a low-resolution study of the metallicity distribution of Leo II. However, their work did not aim at a kinematical analysis of this galaxy and yielded a velocity resolution of 54 km s^{-1} per resolution element (at the region of the CaT) and a median measurement uncertainty of 8.5 km s^{-1}. Hence, and since these authors did not publish individual error estimates of their measurements, we did not include the 37 stars that our observations have in common with their set of 74 red giants in the comparison in Fig. 4. Nonetheless, an analogous fit to that described above above yields $v_{\rm B07} = (0.93 \pm 0.22)\, v_{\rm This\ work} + (12.2 \pm 17.5)$ and a r.m.s. scatter of 10.0 km s^{-1}.

In the light of the respective uncertainties associated with each of the published data sets, there is no significant systematic deviation present in our measurements relative to those from V95 and the results agree to within the errors. On the other hand, there is an indication of a systematic zero point offset of the velocities of Bosler et al. (2007). However, this offset is within the uncertainties and can be attributed to the lower resolution of the latter data set.

3. TESTS FOR APPARENT ROTATION

It is often suggested that the apparent rotation of a system when viewed in projection can be considered as characteristic of tidal perturbation. N-body simulations, (e.g., Oh et al. 1995) indicate that the action of the tidal field of the Galaxy on a dSph leads to velocity gradients in the outer regions of the satellite. When viewed in projection, these dynamical effects will lead to a systematic change in the mean velocity along the dSphs's major axis, thus mimicking rotation (Piatek & Pryor 1995; Oh et al. 1995; Johnston et al. 1995; Mateo et al. 1998; Read et al. 2006a). Hence, the most efficient way of gathering evidence whether a particular dSph is being affected by tides sufficiently strongly that its kinematics are being modified is to look for any sign of apparent rotation in its outer regions. To date, all but one of the dSphs of the Local Group show no significant velocity gradients. The sole exception is Carina, which exhibits some evidence of a difference in the mean velocity at either end of the major axis, for stars beyond the nominal tidal radius (Muñoz et al. 2006).

With its present-day Galactocentric distance of (233$\pm$15) kpc (Bellazzini et al. 2005), Leo II is not expected to have been recently affected by tides, and will only have been perturbed in the past if its orbit brought it into much closer proximity to the Galaxy. This is consistent with its observed regular structure, as pointed out by Coleman et al. (2007). However, since V95 argue that Leo II may not have an unusually high dark matter content compared to the inner Galactic satellites, it cannot be entirely ruled out that it may have been tidally influenced during its evolution despite the presence of a (possibly) considerable amount of dark matter.

In order to investigate the question of tides, we implemented two tests for a significant indication of rotation in the Leo II velocities. First of all, in Fig. 5 we plot the run of radial velocity as a function of major axis distance. In addition, mean radial velocities have been determined in radial bins whose widths were chosen so as to maintain a constant number of stars per bin (lower panel of Fig. 5). If tides had in fact significantly perturbed the outer regions of Leo II, one would expect to see a radial gradient in the velocities. In particular, potential tidal distortions of the galaxy's outskirts, e.g., reflected in tidal tails, could lead to distinct east-west asymmetries in the velocity distributions and one would expect excesses of

[13] We note that the HIRES data of V95, despite their considerably higher spectral resolution than our data, are also of low S/N, which will contribute a non-negligible fraction to the observed scatter in Fig. 4.

high and low velocity stars (w.r.t. the systemic mean) near the outer boundary on opposite sides of the galaxy. It is worth noticing that although 13 of our 200 targeted stars lie outside of the King-tidal radius of 8.7′, only two of these lie within 5σ of the systemic velocity. Recent evidence suggests that Leo II may in fact be slightly more extended, with a nominal tidal radius of 9.2′ (Coleman et al. 2007), but as these values rely strongly on the concept of fitting a particular functional form to surface photometry, such differences remain insignificant and will not be pursued any further in the present work (see Koch et al. 2007a for a detailed discussion). In order to ascertain that we have not missed any potential gradient or high- or low-velocity feature in our data due to our selection criteria, we repeated the averaging in each radial bin after applying several cuts, i.e., at $3\,\sigma$, $5\,\sigma$, and $10\,\sigma$ of the sample mean. For each cut, the data were rebinned to assure a constant number of stars per bin. However, as Fig. 5 implies, there is no significant radial gradient discernible in the kinematics of Leo II for any of the velocity cuts. An error weighted least squares fit to our velocity data yields a slope of $(1.2\pm0.9)\,\mathrm{km\,s^{-1}\,kpc^{-1}}$. Further, those stars with higher and lower velocities than the systemic mean of Leo II are equally distributed across the galaxy and there is no apparent indication of any localized kinematic excess.

To investigate the question of the extent to which any apparent rotational signal in terms of velocity gradients can be excluded, we proceeded a step further and computed the mean radial velocity difference of stars on either side of bisecting lines passing through each individual target. In the presence of a distinct apparent galactic rotation, such a plot should exhibit a clear sinusoidal signal (e.g., Walker et al. 2006; Koch et al. 2007a). These velocity differences are shown in Fig. 6 versus the position angle of the respective bisectors. In fact, there is a peak with an amplitude of $\sim$2 km s^{-1} seen in our data, which is of the same order of magnitude as the radial gradient discussed above. Moreover, the maximum of this distribution occurs at a position angle of $16.5^\circ \pm 2.4^\circ$, where the error was obtained through bootstrap resampling. In the light of the large uncertainty of Irwin & Hatzidimtriou's (1995) quoted systemic position angle, i.e., $(12^\circ \pm 10^\circ)$, we cannot reject a coincidence between the apparent rotational signal in our velocity data and Leo II's minor axis. To assess the actual reality of such a kinematic gradient, we performed 10^4 Monte Carlo runs, in which we generated random samples of velocities at the fixed sky positions of our targets. The velocities for these tests were drawn from a normal distribution, assuming Leo II's mean radial velocity and velocity dispersion, and additionally allowing for a variation by the observed measurement errors. By means of these simulations we find that 87% of the random samples exhibit maximum velocity differences larger than our observed value (Fig. 6, bottom panel). Hence, the apparent rotational signal we detect is only significant at a 13% ($0.17\,\sigma$) confidence level.

As Walker et al. (2006) discuss, apparent rotation can also originate from relative transverse motion of a dSph due to the bulk proper motion of the system. As there are no extant observations of Leo II's proper motion, owing to its large distance, we cannot approach the question of whether the relative motion between the Sun and Leo II would be sufficient to account for the full amplitude of our observed rotation. All in all, there is no kinematical evidence of any significant velocity gradients in Leo II, either due to rotational support or produced by Galactic tides. It therefore appears that tides most likely have not affected Leo II to any significant degree.

4. RADIAL VARIATION OF THE DISPERSION

In order to derive the radial velocity dispersion profile of Leo II we employed a maximum likelihood technique, which is described in more detail in Kleyna et al. (2004) and Koch et al. (2007a). In essence, we radially binned our data such that the same number of stars per bin was maintained. The binsize was defined so as to ensure a sufficiently large number of stars per bin, and we chose to include no fewer than 12 data points in each bin. A Gaussian velocity distribution centered on the single systemic mean velocity is then assumed for each radial bin. This distribution is convolved with the observational errors and also with an additional component, which accounts for the Galactic foreground contamination. The latter is represented by a uniform interloper velocity distribution contributing a fraction f_{int} to each individual bin (see eq. 2 in Koch et al. 2007a). As the velocities of our non-member stars also appear to be well fit by a power-law distribution with an exponent of -0.6, we also considered such an interloper distribution in our determinations of the dispersion profile. Nevertheless, it turned out that the resulting velocity dispersion profiles are indistinguishable in practice and f_{int} is typically compatible with zero in all bins. Finally, the error bounds on the dispersion were calculated by numerically integrating the total probability of the data set and finding the corresponding 68% confidence intervals. Fig. 7 displays the radial dispersion profile thus obtained.

Given the results of Sect. 3, we neglected the effect of a rotationally-induced inflation of the dispersion in our calculations. Another critical issue in the proper dynamical study of a stellar system is the influence of any significant binary population. The presence of any such component in kinematical data leads to an additional, artificial inflation of the observed line of sight velocity dispersion. Furthermore, the high-velocity extension of a binary distribution increases the deviation from a Gaussian so that the assumption of a zero binary fraction yields larger error estimates, which may invalidate the assessment of any radial information derived from the dispersion profiles.

However, it has been shown via Monte Carlo simulations in the past that the influence of binary systems in dSphs is in fact negligible, as the purely binary induced dispersion tends to be small compared to the overall large velocity dispersions found in these galaxies (Hargreaves et al. 1996; Olszewski et al. 1996). Furthermore, repeat observations of red giant velocities in the Draco dSph (Kleyna et al. 2002) and in Fornax (Walker et al. 2006) suggest that the impact of binaries on the measured velocity dispersion is negligible. These kinematical studies did not support an overall binary content larger than 40% in those dSphs. Also, Kleyna et al. (2002) note that the fraction of dynamically significant binaries in the Draco sample amounted to less than 5%. Likewise, Koch et al. (2007a) showed for the case of the Leo I dSph that the as-

sumption of a larger binary fraction does not significantly alter the resulting velocity dispersion profile. Finally, there seems also to be no evidence that binaries would have significantly affected Leo II's internal kinematics, as revealed by the Monte Carlo simulations of V95. If we interpret observed velocity differences as an indication of binarity, there is only one object with a difference in velocity between our measurement and that of V95 that is in excess of 2σ (taken as the measurement uncertainty). If one was to interpret this in terms of binarity (not accounting for any selection effects in the data), this would also suggest a low binary fraction in Leo II. The lack of repeat measurements of the stars in our data set inhibits an assessment of potential binaries. Hence, we will proceed by neglecting the presence of any binary population in our calculations.

The resultant velocity dispersion profile (Fig. 7) is essentially flat out to the last data point and at most subject to fluctuations within the measurement errors. The last point, shown at a median distance of 0.5 kpc in Fig. 7, includes our outermost observed targets at locations of 1.5 kpc from the galaxy's center. Overall, the profile is well described by a constant value of 6.6 $\mathrm{km\,s^{-1}}$, which is in agreement with Leo II's global value derived in Sect. 2.3. Hence it appears that Leo II does in fact show the same behavior as the majority of the dSphs analysed to date, in terms of an essentially flat velocity dispersion profile (Wilkinson et al. 2006 and references therein). This suggests that, similar to the other dSphs, this galaxy is also a dark matter dominated system out to the largest scales. We will turn to the dynamical implications of this finding by deriving Leo II's mass profile and mass to light ratio in Section 5.

4.1. *Correlation with metallicities*

For 52 of the targets around Leo II's velocity peak, metallicities were derived in Paper I. From these it was inferred that Leo II exhibits a wide range of metallicities, covering at least 1.3 dex. The derived age-metallicity relation indicates that Leo II experienced constant star formation over an extended period. Overall, this galaxy appears to have formed stars from 15 Gyr until 2 Gyr ago, although its dominant stellar population is of intermediate age, around 9 Gyr (Mighell & Rich 1996). When split into a metal-poor and a metal-rich population by dividing at the median metallicity, it was shown in Paper I that these stellar components do not differ significantly in their spatial distributions, i.e., there is no apparent metallicity gradient present in Leo II. Moreover, the stellar ages do not appear to show spatial trends. It is then worth noticing that the star formation histories derived from deep, but central, pencil beam surveys such as the HST studies of Mighell & Rich (1996) and Dolphin (2002) are also consistent with our findings in Paper I from a wide-field survey. This again argues in favor of the lack of any considerable population gradient between the center and Leo II's outskirts. In dwarf galaxies with extended star formation histories, the younger and/or more metal-rich populations generally tend to be more centrally concentrated (e.g., Harbeck et al. 2003). Moreover, different stellar populations in dSphs may also have significantly different kinematics, as in the case of Sculptor (Tolstoy et al. 2004) or CVn (Ibata et al. 2006).

In our data, there is no apparent trend of velocity with metallicity discernible (top panel of Fig. 8). In the following, we also separated our velocity data according to their previously assigned metallicities. The respective radial velocity histogram is shown in Fig. 8 (left panel). It turns out that the metal poor stars have slightly higher velocities on average, but the difference between them and the metal richer member candidates is marginal. Using the same formalism as outlined in Section 2.3, we find the mean velocity of the metal poor stars to be $(79.1 \pm 1.6)\,\mathrm{km\,s^{-1}}$ versus $(76.9 \pm 1.0)\,\mathrm{km\,s^{-1}}$ for the metal rich component. The overall velocity dispersions for the two sample are indistinguishable and are consistent with that obtained using the entire velocity data set. In addition, the data were divided into three radial bins (see Fig. 8, right panel). In this case, the metal poor (and presumably older; see Paper I) component has a higher velocity dispersion in each bin. However, given the low number of stars per bin (of order ten at our chosen binning) and the derived measurement uncertainties, any difference in the dispersion between both metallicity populations is in fact insignificant. Thus we conclude that Leo II's stellar populations are kinematically indistinguishable and well-mixed in phase-space, which is fully consistent with the lack of any obvious metallicity or age gradient (Bellazzini et al. 2005; Paper I).

5. MASS, LIGHT AND MASS-TO-LIGHT ESTIMATES

In order to define a mass estimator that can be readily implemented we integrated the Jeans equation (Binney & Tremaine 1998, eqs. 4-54 ff.; Koch et al. 2007a) under the assumption of spherical symmetry and an isotropic velocity distribution. Since our data cover the entire face of the galaxy, this procedure has the advantage of exploiting the full kinematic information that has been gathered in the previous sections as opposed to mass estimates that rely on the single value of a central velocity dispersion (e.g., V95; Coleman et al. 2007 for the case of Leo II). Moreover, these methods of "core-fitting" make the assumption that the mass distribution follows that of the light (Richstone & Tremaine 1986; V95), which has been shown to be invalid in the case of the Draco dSph (Kleyna et al. 2002). Nevertheless, a limitation of the simple formalism employed in this section is the neglect of the degeneracy between velocity dispersion and anisotropy (Wilkinson et al. 2002), which persists unless large data sets and/or higher moments of the velocity distribution are considered (e.g., Binney & Mamon 1982; Łokas & Mamon 2003). We will account for this effect in detail in Sect. 6.

The surface brightness profile required for the mass determinations was adopted from a fit to the data of Irwin & Hatzidimitriou (1995). It is well fit by a Plummer profile with a characteristic radius of $2.76' \pm 0.09'$ (see Fig. 9), where the error was determined via bootstrap resampling (e.g., Mackey & Gilmore 2003). This value is in fact very similar to Leo II's core radius from a King (1966) profile fit (Irwin & Hatzidimitriou 1995; Coleman et al. 2007) and use of the latter value yields analogous results for the mass computations. As implied by the results from the previous sections the dispersion profile was assumed to be radially constant.

The resultant mass profile of Leo II is shown in Fig. 9. From this we estimate its total mass out to the tidal radius

at 8.7′ (0.6 kpc) to be $(2.7 \pm 0.5) \times 10^7\,M_\odot$. The quoted errors were obtained from a Monte Carlo simulation of the mass calculation and take into account the 1σ confidence interval of the velocity dispersion as well as the uncertainty in the parameters of the light profile.

Also shown in Fig. 9 is the density profile that we obtained from the above dynamical considerations. It is characterised by a central density of $\rho_0 = (3.4 \pm 0.4) \times 10^8\,M_\odot\,\mathrm{kpc}^{-3}$, which is in good agreement with the value of $(4.0 \pm 1.1) \times 10^8\,M_\odot\,\mathrm{kpc}^{-3}$ derived by V95 from their analysis of Leo II's very center.[14] Leo II's density distribution resembles a cored profile in the innermost regions, although we note that our innermost target star lies at a distance of 0.5′ (0.03 kpc) from the center so that any assessment of the "central" density has to rely on an extrapolation. The profile reaches a power-law slope of -1 at approximately 0.13 kpc and converges towards a slope of -2 for distances larger than 0.5 kpc.

With these mass estimates at hand, we derive the satellite's M/L ratio by adopting its luminosity from the literature. Thence the (M/L) (in solar units) varies from $26.6^{+5.5}_{-4.5}$ for $L_V = (9.9 \pm 0.2) \times 10^5\,L_\odot$ (V95), $35.6^{+8.8}_{-7.7}$ ($L_V = (7.4 \pm 2.0) \times 10^5\,L_\odot$; Coleman et al. 2007) to $45.4^{+11.7}_{-10.4}$ for $L_V = (5.8 \pm 1.8) \times 10^5\,L_\odot$ (Mateo 1998)[15]. In all cases, a M/L of this order of magnitude strongly suggests that Leo II is governed by a considerable amount of dark matter on all spatial scales. Mateo et al. (1998) estimate that the *stellar* $(\mathrm{M/L})_V$ for a galaxy like Leo II with prominent old and intermediate age populations (see also Paper I) is of the order of 1–1.4. If, on the other hand, Leo II contained only an old, single-age globular cluster-like stellar population, then Mateo et al. (1998) indicate that the M/L ratio of Leo II would be higher than the value of the galaxy's actual population by a factor of ∼1.3. Clearly, these results and our observations show that the dark matter content of Leo II is well above that expected in a purely old stellar population. From their photometric structural analysis of Leo II, Coleman et al. (2007) derive its M/L via two assumptions: for the case of mass follows light they end up with a $(\mathrm{M/L})_V$ of 7, whereas for the other extreme of a pure dark matter dominance, this value may be as high as ∼125. The fact that our full kinematical analysis points towards the higher end of these directions underscores the dark matter dominated state of Leo II, with at most mild tidal perturbation. Since the spatial resolution of our data and the resulting method is an improvement over the traditional core-fitting methods, which assume a constant M/L, we show in Fig. 9 (bottom panel) also the theoretical M/L profile over the full range covered by our observations and using the previously derived parameters. Already at Leo II's center the M/L is an order of magnitude higher than the purely stellar estimates.

Given the above results, Leo II fits well remarkably well on the (M/L) versus M_V relation for dSphs (see Fig. 5 in Gilmore et al. 2007), which is an oft-used argument in favor of all dSphs being embedded in dark halos of the same mass. Although the exact value of such a common mass scale is subject to various assumptions such as the M/L of the pure stellar component, this underlying halo tends to be of the order of $3 \times 10^7\,M_\odot$ (Mateo et al. 1993; Wilkinson et al. 2006; Gilmore et al. 2007).

6. VELOCITY ANISOTROPY – CUSP VERSUS CORE

All the mass computations in Sect. 5 relied on the assumption of an isotropic velocity tensor, i.e., the anisotropy parameter $\beta = 1 - \langle v_\theta^2 \rangle / \langle v_r^2 \rangle$ was assumed to be zero. Nonetheless, there is compelling evidence that the shapes and kinematics of most dSphs necessitate non-negligible amounts of velocity anisotropy on all spatial scales (e.g., Łokas 2002; Kleyna et al. 2002; Wilkinson et al. 2004; Klimentowski et al. 2007). As the neglect of a non-isotropic velocity distribution can considerably affect estimates of the underlying dark halo mass, we explore in the following the possible parameter space of Leo II's velocity anisotropy. In doing this we follow the same formalism as outlined in Koch et al. (2007a) (see also Łokas 2002). That is, under the assumption of a (constant) anisotropy parameter and for different plausible mass profiles, we numerically determined a theoretical velocity dispersion profile; the model parameters were then optimized in a least-squares sense to yield the best representation of the observations from Sect. 4.

6.1. *Density cusps*

Motivated by the cosmological simulations of Navarro, Frenk & White (1995; NFW), the density profiles of dark matter halos are often described by a convenient function with only one free parameter, the "characteristic density". For simulated haloes, this parameterisation has proven applicable to a wide range of halo masses from the smallest scales, such as the dSphs' dark matter associations, up to the large scale structures of galaxy clusters. We first adopted this cuspy halo mass model,

$$M(r) \;\propto\; M_v \left\{ \ln(1 + cr/r_v) \;-\; \frac{cr/r_v}{1 + cr/r_v} \right\}, \qquad (1)$$

in our computations of an empirical dispersion profile. In our representation, the only free parameter is the virial halo mass, M_v, and all other parameters, namely virial radius r_v and concentration c, are empirically scaled with this mass according to the relations obtained by Jing & Soto (2000) (see Łokas & Mamon 2001; eqs. 9–12 in Koch et al. 2007a for details of the parameterisations).

The best-fit results for varying degrees of anisotropy are overlaid on the observed dispersion profiles in Fig. 10. For all choices of β, the virial mass of the NFW-halo is of the order $2.3 \times 10^8 M_\odot$, corresponding to a formal virial radius of about 12 kpc (which is much larger than the stellar limiting radius, allowing for the factor of ∼10 in mass out to the virial radius). As for the anisotropy parameter, the reduced χ^2 for a β of $(-1, -0.5, 0, 0.5)$ amounts to (0.29, 0.21, 0.22, 0.47). The best coincidence of prediction and observation is obtained when a slight amount of tangential anisotropy ($\beta \sim -0.25$) is included.

6.2. *Cored density profile*

[14] Coleman et al. (2007) yield a lower value of $\rho_0 = (1.3 \pm 0.4) \times 10^8\,M_\odot\,\mathrm{kpc}^{-3}$ under the assumption of a Gaussian mass and light distribution.

[15] For the subsequent discussions of Leo II's M/L, e.g., Gilmore et al. (2007), we adopt the latter value using Mateo's (1998) luminosity estimate, since this value is, in turn, based on the measurements of Irwin & Hatzidimitriou (1995), whose surface brightness profile we employed.

The majority of presently available observational data of low-luminosity galaxies indicates that their kinematics and structures are consistent with cored density profiles (e.g., Łokas 2002; Kleyna et al. 2003; Salucci et al. 2003; Sánchez-Salcedo et al. 2006). Hence, we also computed dispersion profiles in the same manner as above for a halo profile with variable inner logarithmic slope (Hernquist 1990; Read & Gilmore 2005; eq. 13 in Koch et al. 2007a):

$$\rho(r) \propto C \left(\frac{r}{r_s}\right)^{-\gamma} \left[1+\left(\frac{r}{r_s}\right)^{\alpha}\right]^{(\gamma-3)/\alpha} \quad (2)$$

The parameters were then determined such as to match the observed dispersion profile for different values of the anisotropy β.

As it turns out, the "best-fit" for all choices of anisotropy was obtained for a slope parameter of $\gamma \simeq 0$, which corresponds to a pure core, as opposed to the cuspy halo class ($\gamma = 1$). Moreover, a scale radius r_s of 0.3 kpc and a large smoothness parameter α (which determines the sharpness of the transition toward the density profile at large radii) of ∼3.7 were found to yield the best representation of our data (see lower panels of Fig. 10). For this cored model, the values of the reduced χ^2 are (0.21, 0.20, 0.21, 0.31) for constant anisotropies of (−1, −0.5, 0, 0.5) and, as for the cuspy halos, our data ideally require some tangential anisotropy of the same order of magnitude, that is $\beta \sim -0.25$.

It is worth noticing that our data do not allow us to unequivocally constrain the shape of the velocity anisotropy tensor at large radii for either choice of halo profile. However, we can conclude from Fig. 10 that strongly radial anisotropy is not suitable to account for the dispersion profile towards the central regions.

6.3. *Cusp or Core ?*

For both profiles investigated above, the mass at the galaxy's limiting radius amounts to $\sim 2.0 \times 10^7 M_\odot$ and is thus slightly smaller than that derived from a purely isotropic velocity distribution in Sect. 5[16].

Judging by the values of the χ^2 statistics, a cored density profile is favored to account for the Leo II observed kinematics; however, the difference between this and the cuspy model is small. In particular, there is an indication of a leveling off of the predictions for the dispersion towards larger radii for the cored model, a trend that merits further investigation from a large sample of stars at and beyond the limiting radius of this galaxy.

In addition, we re-ran the computations with a velocity anisotropy which varies radially according to the prescription of Osipkov (1979) and Merritt (1985), i.e., $\beta(r) = r^2/(r^2 + r_a^2)$, which yields radial anisotropy for the case of $r > r_a$. The resulting curves are shown in the right panels of Fig. 10. While the NFW halo requires an anisotropy radius r_a of ∼0.7 kpc and thus larger than Leo II's tidal radius, the cored profile is best associated with a r_a of ∼0.2 kpc. The respective χ^2 statistics are then 0.22 and 0.19, thus again marginally favoring a cored halo[17]

As a comparison with extant data of the density profiles of Local Group dSphs indicates, the majority of these systems are consistent with cored inner halo profiles, which is similar to our findings for Leo II (Wilkinson et al. 2006; Gilmore et al. 2007 – see their Fig. 4). While the outer density profile of Leo II is similar to those of the other LG dSphs analysed to date, Leo II apparently exhibits a mildly steeper central density profile than the other dwarfs, due to the apparently smaller size of its central core.

From their photometric analysis Coleman et al. (2007) argue that Leo II's M/L ratio has an upper limit of 125^{+56}_{-51} under the assumption of a constant density core out to their tidal radius. Although our value derived in the previous Section is lower by a factor of approximately 3, we note that the core size we obtain in the density profile is correspondingly smaller.

7. SUMMARY

We have obtained a large data set of radial velocity measurements for about 171 red giant member candidates in the remote Leo II dSph, thereby increasing existing published samples more than fivefold (V95). These data extend in radial distance out to the galaxy's limiting radius, which is an important prerequisite for kinematic studies, since Leo II, as the second most remote dSph satellite of the Milky Way, is valuable for an assessment of the potential role of Galactic tides. With its moderate present-day systemic velocity, Leo II can be considered as bound to the Galaxy and yet there is no indication of any tidal perturbation. This lack of perturbations is expected if this dSph has maintained its present large distance over long time-scales. Our study precludes any apparent rotation of Leo II's stellar component; moreover we do not detect a velocity gradient, nor any asymmetry in the sense that high and low velocity outliers preferentially reside in particular directions along the major axis, which might reflect the action of tides. Although other dSphs may well exhibit "extratidal" material (e.g., Carina; Muñoz et al. 2006) or be in an advanced state of dissolution (e.g., Sagittarius; Ibata et al. 1994), these effects are clearly not seen in Leo II. Thus we must conclude that this galaxy is a purely pressure-supported system which has not been significantly affected by tides over the course of its evolution.

The radial velocity dispersion profile and resulting density profiles show a resemblance to the respective profiles of the majority of the other Local Group dSphs, and display the well-established features of these systems, namely a dispersion which is flat out to the reach of the present data and a density profile that is consistent with a cored halo mass distribution. We note, however, that our present data do not unambiguously distinguish between the possibilities of a cusped or cored density profile in terms of the χ^2-statistics of the best-fit to our observed dispersion profile. Both cored and cusped halo models favor the presence of a mild amount of tangential velocity anisotropy in the central regions of the galaxy.

All in all, we find that Leo II is a typical dSph in terms of the values of its total mass of $\sim 3\times10^7\,M_\odot$ and of its characteristic central density of the order of $3.4\times10^8\,M_\odot\,\mathrm{kpc}^{-3}$

[16] The assumption of velocity isotropy would generally lead to an overestimate of the mass at large radii, if Leo II were indeed tangentially anisotropic, whereas if it were radially anisotropic in the outer parts, we would underestimate the mass assuming isotropy.

[17] We note that a radially varying tangential anisotropy $\beta(r) = r^2/(r^2 - r_a^2)$ (Merritt 1985; his model II) yields essentially the same results.

(Gilmore et al. 2007). Depending on the adopted total luminosity of Leo II, we estimate its M/L ratio to lie in the range 25 to 50. This is, in conjunction with the flatness of the dispersion profile, striking evidence that Leo II is a dark matter dominated system. Moreover, the value we find is consistent with the idea that all dSphs are embedded in a dark matter halo with one single characteristic mass scale. Taking into account that all nearby dSph galaxies contain very old stellar populations (Grebel & Gallagher 2004), it thus appears reasonable to consider these objects as the smallest surviving condensations of dark matter with associated stellar populations in the universe (Read et al. 2006b).

A.K. and E.K.G. are grateful for support by the Swiss National Science Foundation through grants 200020-105260 and 200020-113697. M.I.W. acknowledges the Particle Physics and Astronomy Research Council and the Royal Society for financial support.

REFERENCES

Aaronson, M. 1983, ApJ, 266, L11
Bellazzini, M., Gennari, N., & Ferraro, F. R. 2005, MNRAS, 360, 185
Belokurov, V., et al., 2006, ApJ, 647, L111
Belokurov, V., et al., 2007, ApJ, 654, 897
Binney, J., Mamon, G. A. 1982, MNRAS, 200, 361
Binney, J., & Tremaine S. 1998, "Galactic Dynamics", Princeton University Press
Blecha, A., Cayatte, V., North, P., Royer, F., & Simond, G. 2000, Data-reduction software for GIRAFFE, the VLT medium-resolution multi-object fiber-fed spectrograph, in Optical and IR Telescope Instrumentation and Detectors, ed. I.Masanori, & A.F.Moorwood, SPIE, 4008, 467
Bosler, T. L., Smecker-Hane, T. A., & Stetson, P. B. 2007, MNRAS, submitted (astro-ph/0608197)
Chapman, S. C., Ibata, R., Lewis, G. F., Ferguson, A. M. N., Irwin, M., McConnachie, A., & Tanvir, N. 2005, ApJ, 632, L87
Colafrancesco, S., Profumo, S., & Ullio, P. 2007, Phys. Rev. D, 75, 023513
Coleman, M. C., Jordi, K., Koch, A., Grebel, E. K. & Rix, H.-W., 2007, AJ, submitted
Diemand, J., Zemp, M., Moore, B., Stadel, J., & Carollo, C. M. 2005, MNRAS, 364, 665
Dolphin, A. E. 2002, MNRAS, 332, 91
Gentile, G., Salucci, P., Klein, U., Vergani, D., & Kalberla, P. 2004, MNRAS, 351, 903
Gilmore, G., Wilkinson, M. I., Kleyna, J. T., Wyse, R. F. G., Koch, A., Evans, N. W., & Grebel, E. K. 2007, ApJ, in press (astro-ph/0703308)
Goerdt, T., Moore, B., Read, J. I., Stadel, J., & Zemp, M. 2006, MNRAS, 368, 1073
Grebel, E. K., Gallagher, J. S., & Harbeck, D. R. 2003, AJ, 125, 1926
Grebel, E. K., & Gallagher, J. S., ApJ, 610, L89
Hargreaves, J. C., Gilmore, G., & Annan, J. D. 1996, MNRAS, 279, 108
Hernquist, L. 1990, ApJ, 356, 359
Ibata, R. A., Gilmore, G., & Irwin, M. J. 1994, Nature, 370, 194
Ibata, R. Chapman, S., Irwin, M., Lewis, G., & Martin, N. 2006, MNRAS, 373, L70
Irwin, M. & Hatzidimitriou, D. 1995, MNRAS, 277, 1254
Irwin, M., & Lewis, J. 2001, New Ast. Rev., 45, 105
Irwin, M., et al., 2007, ApJ, 656, L13
Jing, Y. P., & Suto, Y. 2000, ApJ, 529, L69
Johnston, K. V., Spergel, D. N., & Hernquist, L. 1995, ApJ, 451, 598
King, I. R. 1966, AJ, 71, 64
Klessen, R. S., & Zhao, H. 2002, ApJ, 566, 838
Klessen, R. S., Grebel, E. K., & Harbeck, D. R. 2003, ApJ, 589, 798
Kleyna, J. T., Wilkinson, M. I., Evans, N. W., Gilmore, G.F., & Frayn, C. 2002, MNRAS, 330, 792
Kleyna, J. T., Wilkinson, M. I., Gilmore, G., & Evans, N. W. 2003, ApJ, 588, L21
Kleyna, J. T., Wilkinson, M. I., Evans, N. W. & Gilmore, G. F. 2004, MNRAS, 354, L66
Klimentowski, J., Łokas, E. L., Kazantzidis, S., Prada, F., Mayer, L., & Mamon, G. A. 2007, MNRAS, subm. (astro-ph/0611296)
Koch, A., Grebel, E. K., Wyse, R. F. G., Kleyna, J. T., Wilkinson, M. I., Harbeck, D. R., Gilmore, G. F., & Evans, N. W. 2006, AJ, 131, 895
Koch, A., Wilkinson, M.I., Kleyna, J.T., Gilmore, G.F., Grebel, E.K., Mackey, D., & Evans, N.W., & Wyse, R.F.G. 2007a, ApJ, 657, 241
Koch, A., Grebel, E. K., Kleyna, J. T., Wilkinson, M. I., Harbeck, D. R., Gilmore, D. R., Wyse, R. F. G., & Evans, N. W. 2007b, AJ, 133, 270; (Paper I)
Kroupa, P., 1997, New Astronomy, 2, 139
Kuhn, J. R., Miller, R. H., 1989, ApJ, 341, L41
Łokas, E. L., & Mamon, G. A. 2001, MNRAS, 321, 155
Łokas, E. L. 2002, MNRAS, 333, 697
Łokas, E. L., & Mamon, G. A. 2003, MNRAS, 343, 401
Mateo, M., Olszewski, E. W., Pryor, C., Welch, D. L., & Fisher, P. 1993, AJ, 105, 510
Mackey, D. A., & Gilmore, G. F. 2003, MNRAS, 338, 85
Mateo, M. 2005, in IAU Colloquium 198, Near-field cosmology with dwarf elliptical galaxies, ed. H. Jerjen & B. Binggeli (Cambridge: CUP), 52
Mateo, M. 1998, AR&A, 36, 435
Mateo, M., Olszewski, E. W., Vogt, S. S., & Keane, M. J. 1998, AJ, 116, 2315
Merrit, D. 1985, AJ, 90, 1027
Mighell, K. J., & Rich, R. M. 1996, AJ, 111, 777
Muñoz, R. R., et al. 2006, ApJ, 649, 201
Navarro, J. F., Frenk, C. S. & White, S. D. M. 1995, MNRAS, 275, 720 (NFW)
Odenkirchen, M., et al. 2001, AJ, 122, 2538
Oh, K. S., Lin, D. N. C., & Aarseth, S. J. 1995, ApJ, 442, 142
Olszewski, E. W., Pryor, C., Armandroff, T. E. 1996, AJ, 111, 750
Osipkov, L. P. 1979, Pis'ma Astron. Zh., 5, 77
Palma, C., Majewski, S. R., Siegel, M. H., Patterson, R. J., Ostheimer, J. C. & Link, R. 2003, AJ, 125, 1352
Pasquini, L., et al. 2002, The ESO Messenger, 110, 1
Piatek, S., & Pryor, C. 1995, AJ, 109, 1071
Read, J. I., & Gilmore, G. 2005, MNRAS, 356, 107
Read, J. I., Wilkinson, M. I., Evans, N. W., Gilmore, G., Kleyna, J. T. 2006a, MNRAS, 367, 387
Read, J. I., Wilkinson, M. I., Evans, N. W., Gilmore, G., Kleyna, J. T. 2006b, MNRAS, 366, 429
Richstone, D. O., & Tremaine, S. 1986, AJ, 92, 72
Robin, A. C., Reylé, S., Derrière, S., & Picaud, S. 2003, A&A, 409, 523
Salucci, P., Walter, F., & Borriello, A. 2003, A&A, 409, 53
Sánchez-Salcedo, F. J., Reye-Iturbide, J., & Hernandez, X. 2006, MNRAS, 370, 1829
Segall, M., Ibata, R., Irwin, M., Martin, N., & Chapman, S. 2007, MNRAS, 375, 831
Spekkens, K., Giovanelli, R., & Haynes, M. P. 2005, AJ, 129, 2119
Strigari, L. E., Bullock, J. S., Kaplinghat, M., Kravtsov, A. V., Gnedin, O. Y., Abazajian, K., & Klypin, A. A. 2006, ApJ, 652, 306
Tolstoy, E., et al. 2004, ApJ, 617, L119
Tonry, J. L., & Davis, M. 1979, AJ, 84, 1511
Vogt, S. S., Mateo, M., Olszewski, E. W., & Keane, M. J. 1995, AJ, 109, 151 (V95)
Walker, M. G., Mateo., M., Olszewski, E. W., Bernstein, R. A., Wang, X., & Woodroofe, M. 2006, AJ, 131, 2114
Westfall, K. B., Majewski, S. R., Ostheimer, J. C., Frinchaboy, P. M., Kunkel, W. E., Patterson, R. J., & Link, R. 2006, AJ, 131, 375
Wilkinson, M. I., Kleyna, J., Evans, N. W., Gilmore, G., 2002, MNRAS, 330, 778
Wilkinson, M. I, Kleyna, J. T., Evans, N. W., Gilmore, G., Irwin, M. J., & Grebel, E. K. 2004, ApJ, 611, L21
Wilkinson, M. I., Kleyna, J. T., Evans, N. W., Gilmore, G. F., Read, J. I., Koch, A., Grebel, E. K., & Irwin, M. J. 2006, in EAS Publications Series 20, Mass Profiles and Shapes of Cosmological Structures, ed. G.A. Mamon, F. Combes, C. Deffayet, & B. Fort (Paris: EDP Sciences), 105
Wu, X. 2007, AJ, subm. (astro-ph/0702233)
Wyse, R.F.G., Gilmore, G.F., Norris, J.E., Wilkinson, M.I., Kleyna, J.T., Koch, A., Evans, N.W., & Grebel, E.K. 2006, ApJ, 639, L13
Zucker, D. B., et al. 2006, ApJ, 643, L103
Zucker, D. B., et al. 2006, ApJ, 650, L41

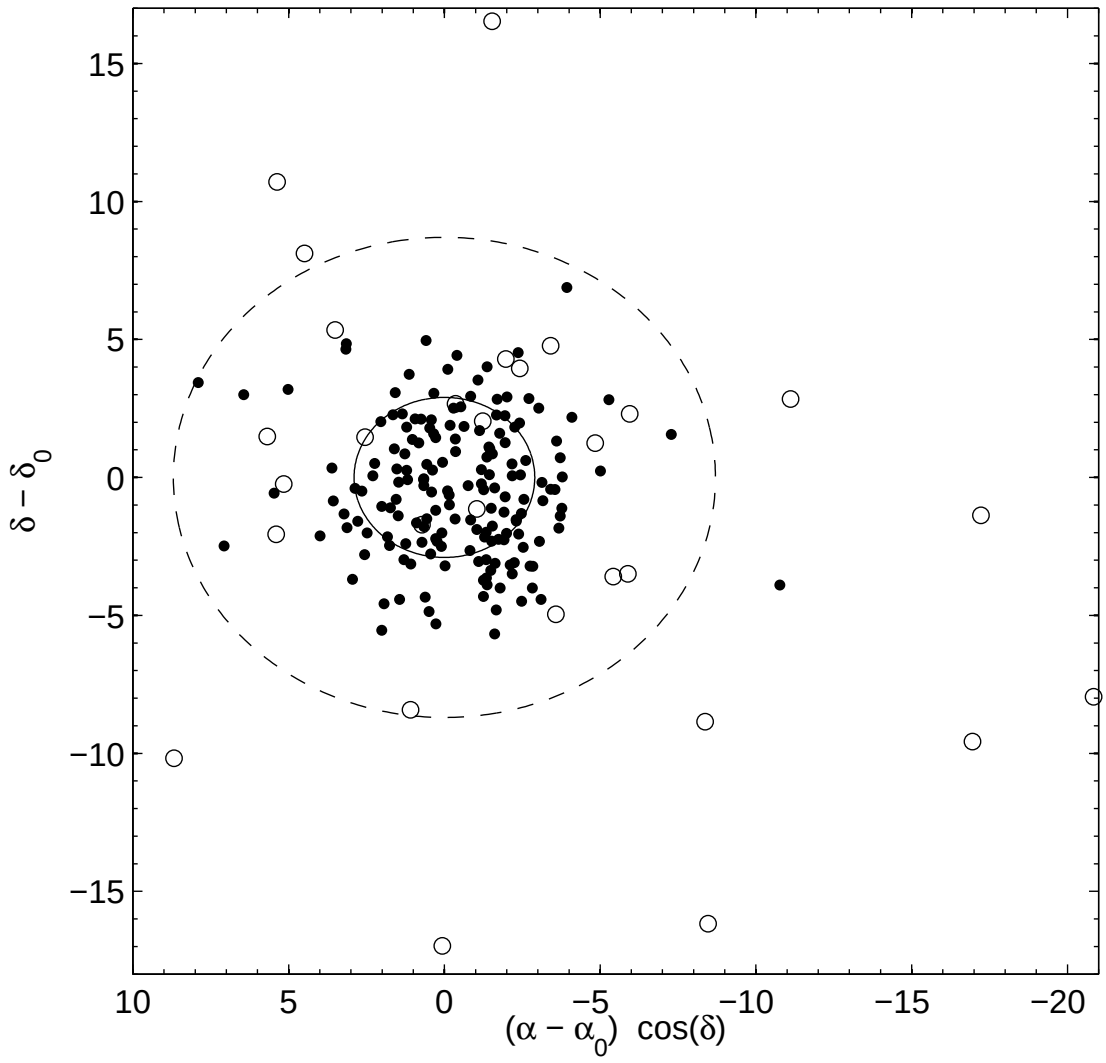

FIG. 1.— Distribution of our targets on the sky, centered on Leo II. Apparent radial velocity non-members are designated with open circles. The solid and dashed lines indicate Leo II's core and nominal King tidal radius at 2′.9 and 8′.7 (Irwin & Hatzidimitriou 1995).

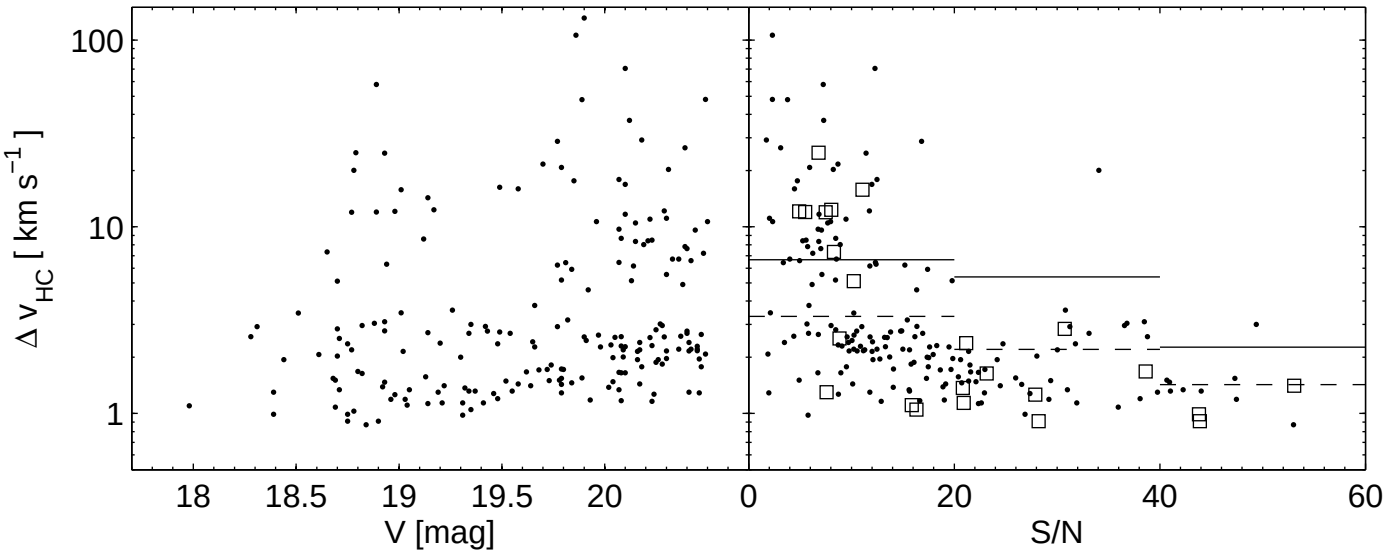

FIG. 2.— Velocity errors versus V-band magnitude (left panel) and Signal to Noise ratio per pixel (right panel). The dashed lines in the right panel indicate our formal mean velocity errors in each S/N bin, whereas the solid lines show the r.m.s. discrepancy between our measurements and those of V95 (open squares), which we use to re-scale our uncertainties in Sect. 2.4.

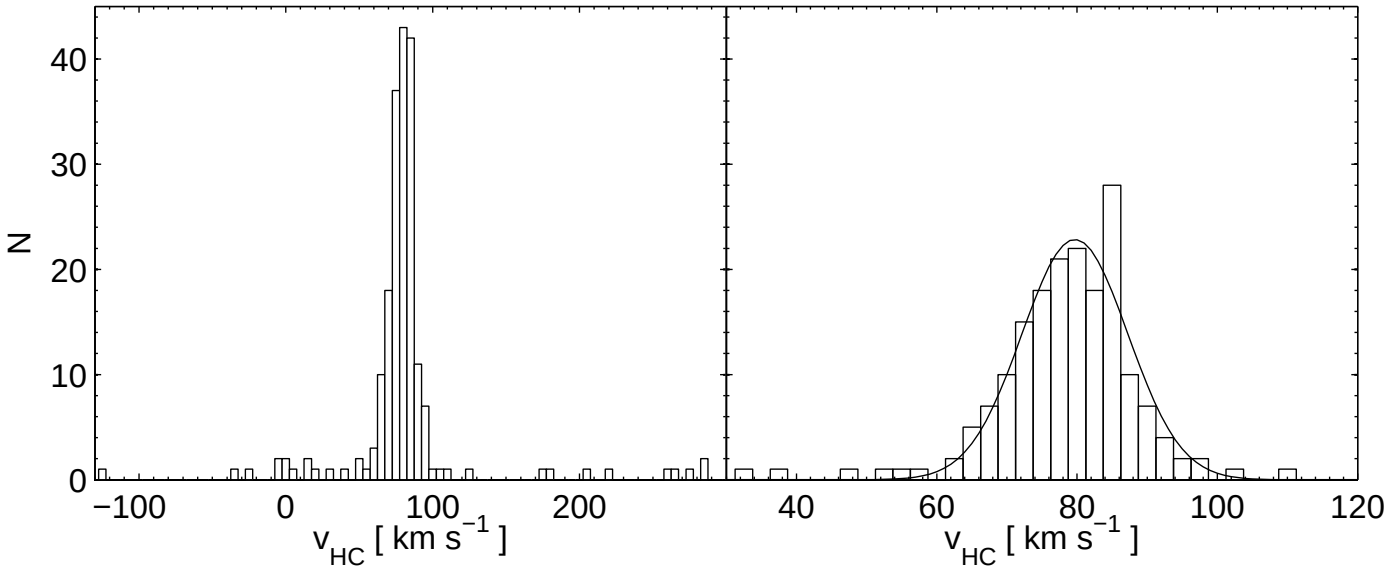

FIG. 3.— Histograms of the radial velocities of stars in our survey of Leo II. The left panel displays the full sample, whereas the right panel only shows stars around Leo II's systemic velocity. The best-fit Gaussian to this distribution is shown as a solid line.

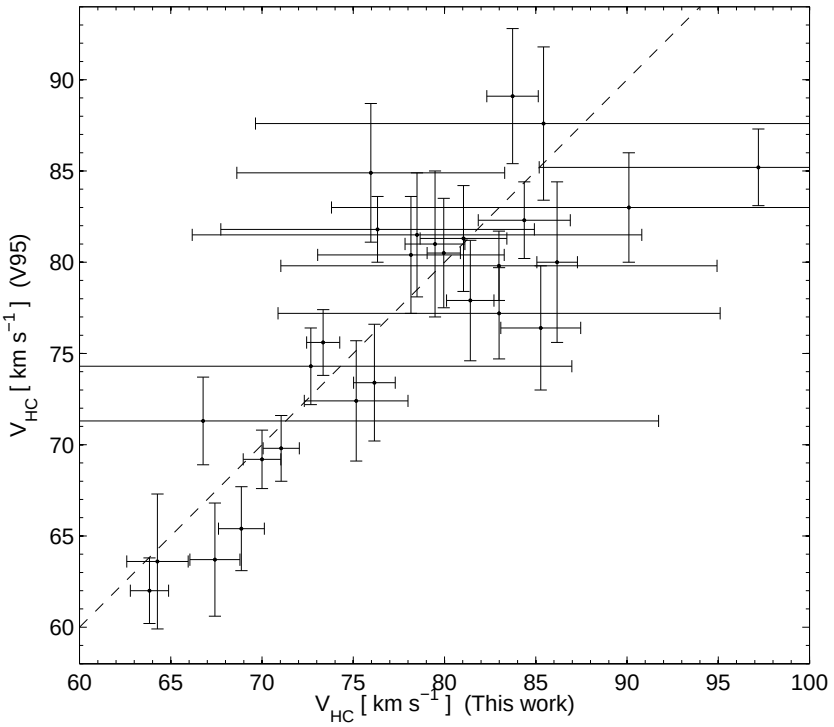

FIG. 4.— Comparison of our velocity measurements to those estimated by Vogt et al. (1995) for the 28 stars in common between the two data sets. The scale factors to the error bars have not been applied in this diagram to illustrate our internal formal measurement errors. The dashed line is unity.

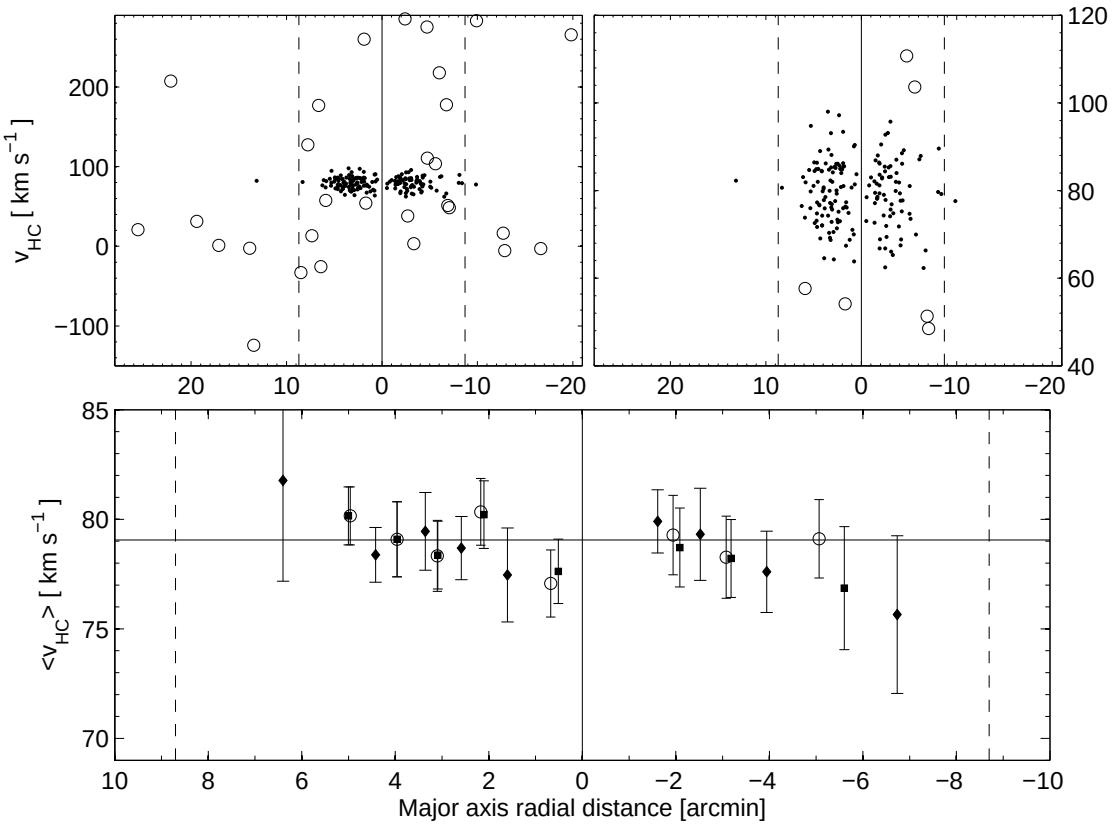

FIG. 5.— Top panels: Radial velocity versus major axis radial distance. The right panel shows those stars around Leo II's mean systemic velocity, while the full data are included in the left panel. Members within (outside) a $3\,\sigma$ cut are shown as filled (open) symbols. The bottom panel displays mean radial velocities obtained in radial bins with a constant number of stars, where we adopted different cuts in velocity to consider the presence of high- or low-velocity member stars: $3\,\sigma$ (open circles), $5\,\sigma$ (solid squares), and $10\,\sigma$ (filled diamonds). No significant radial gradient is discernible in our data. Monte Carlo tests show that the hint of a change in the mean velocity between the outer bins at each end of the major axis is not statistically significant (see text for details). Note the different scales in each of the subplots.

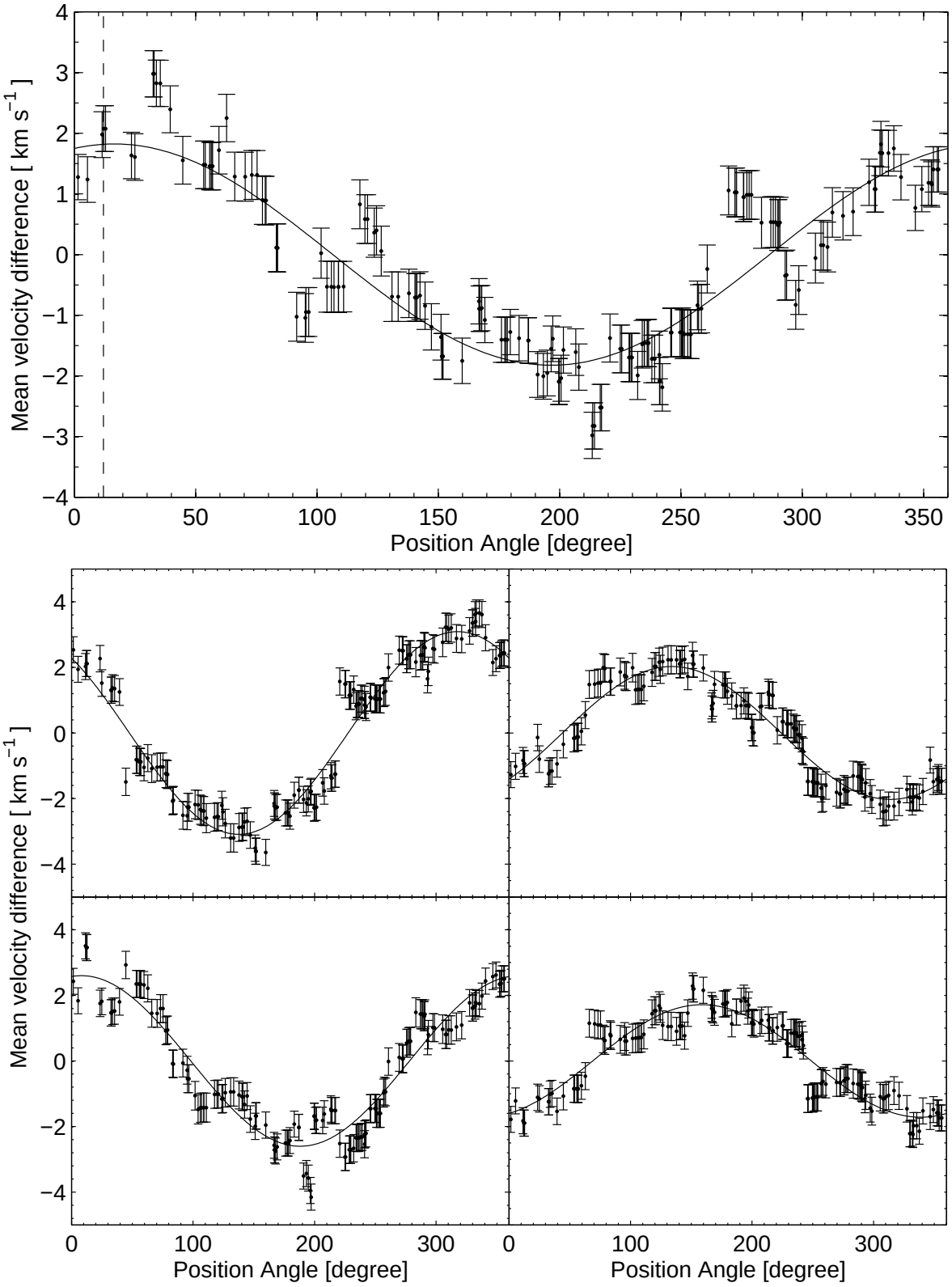

FIG. 6.— Test for apparent rotation in our observations (top panel) and a sample of Monte Carlo simulations (bottom panel). The points with error bars show the mean velocity difference of stars on either side of bisecting lines at the respective position angles. The best-fit sinusoid is displayed as a solid line. The discernible rotation amplitude at a position angle of ∼23° is statistically insignificant – 87% of the random samples as shown in the bottom panel produce a comparable amplitude or larger. Indicated as a dashed line in the top panel is the minor axis position angle of 12° from Irwin & Hatzidimitriou (1995).

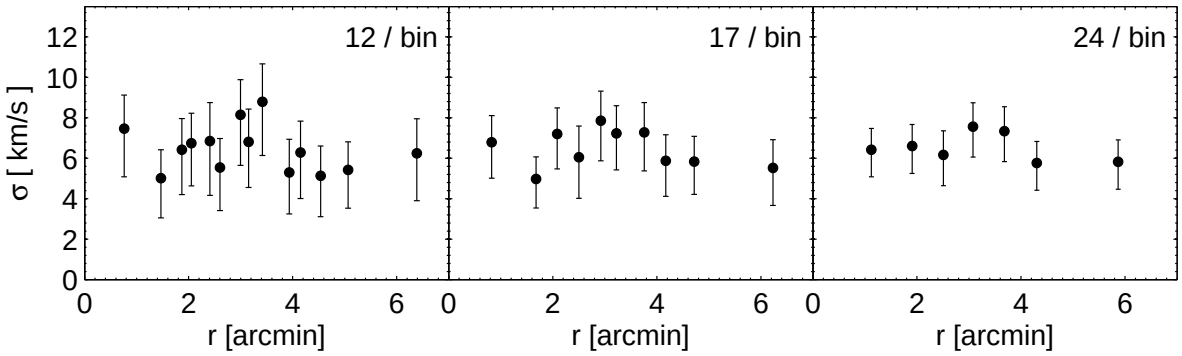

FIG. 7.— Leo II's radial velocity dispersion profile obtained for a $3\,\sigma$ membership criterion. In each panel, each bin contains the indicated constant number of stars.

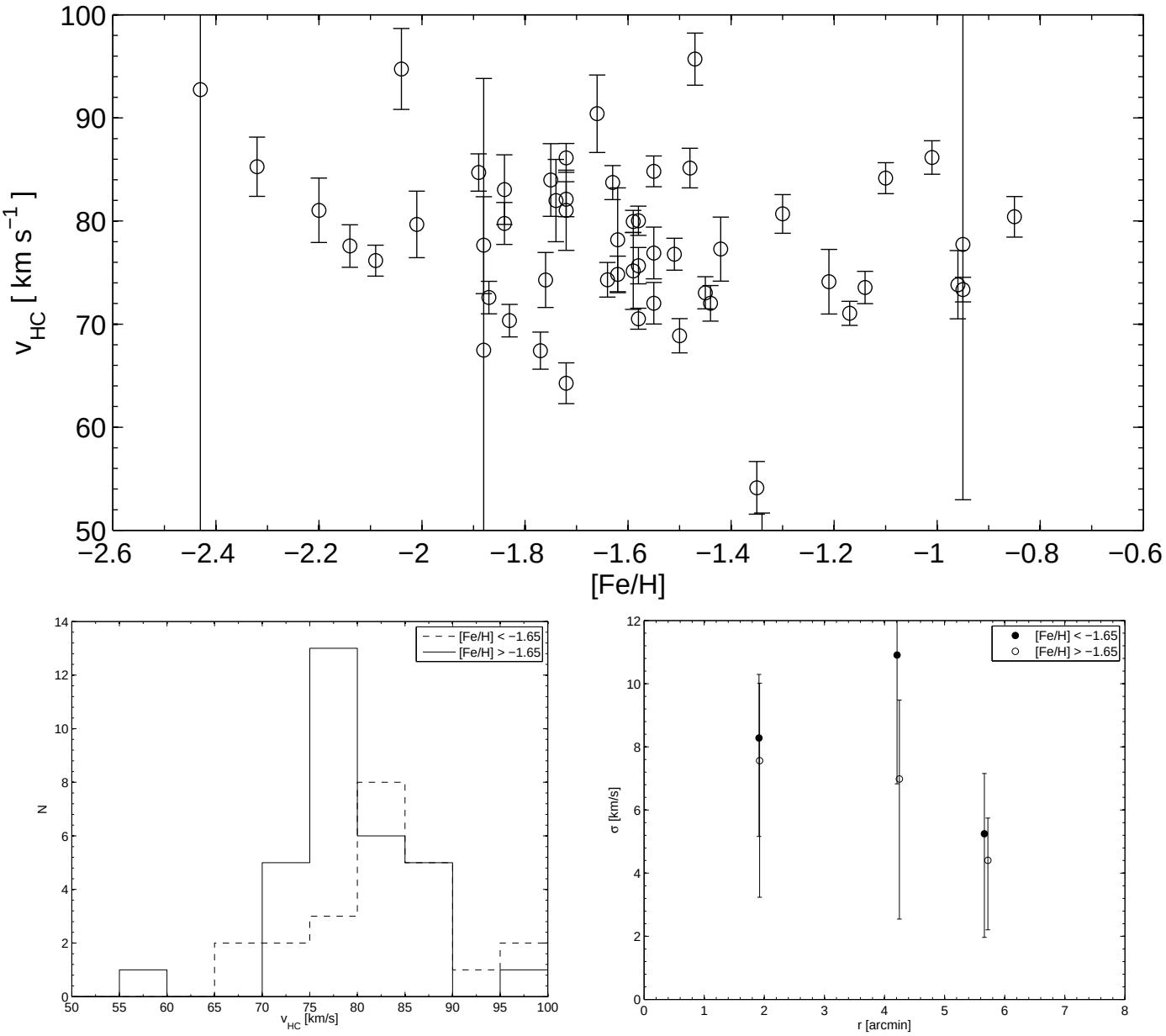

FIG. 8.— Upper panel: Velocity distribution for a subsample of our data for which there is extant metallicity information (Paper I). The velocity histograms and dispersion profiles in the lower panels have been separated into a metal-poor and a metal-rich component, which exhibit only marginally different kinematics.

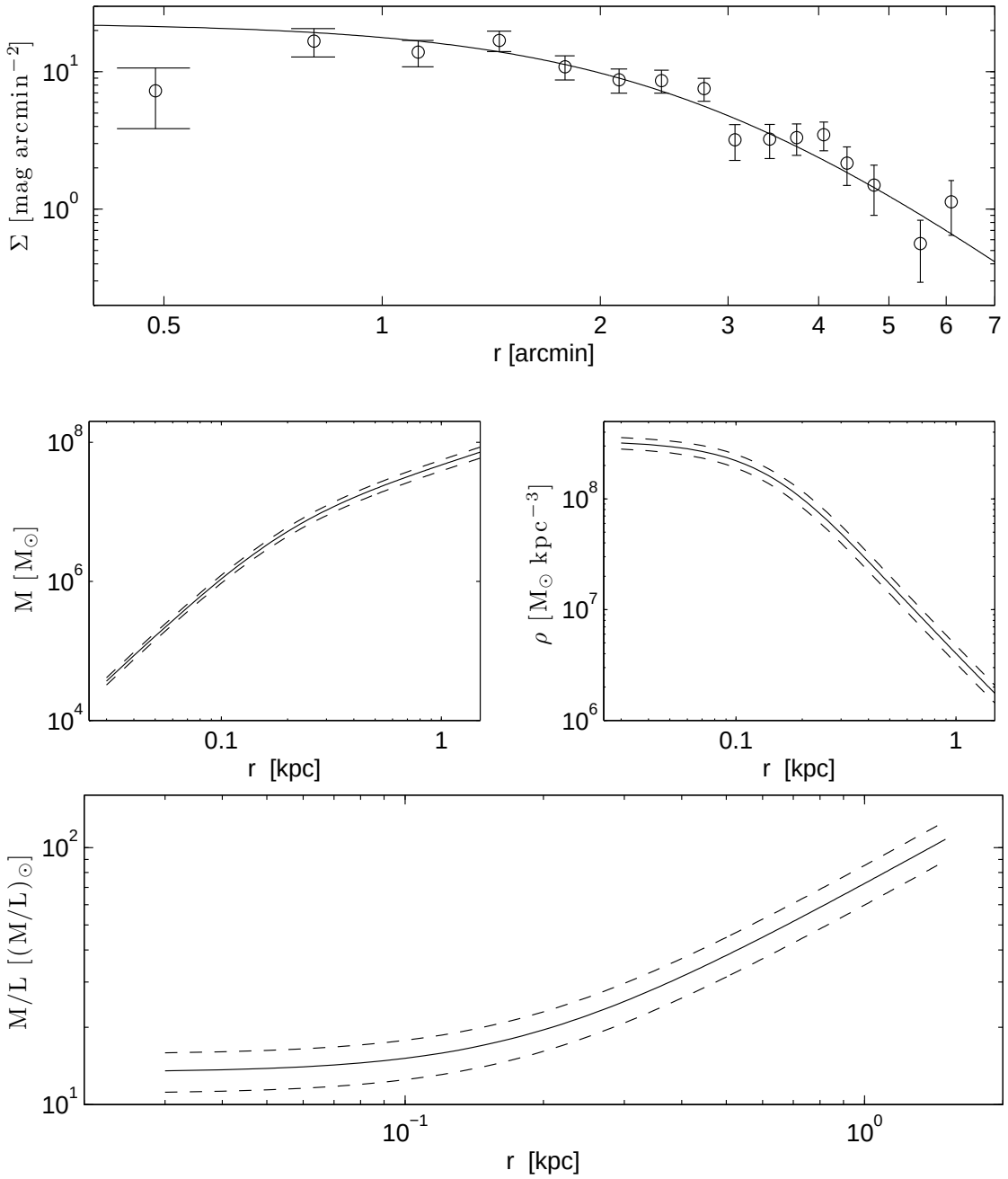

FIG. 9.— Mass (middle left panel) and density (middle right) profile of Leo II, obtained from Jeans equation under the assumption of an isotropic velocity distribution and a constant velocity dispersion. Error bounds originate from the uncertainties in the light and velocity dispersion profile. The surface brightness profile entering the calculations is shown in the top panel (after Irwin & Hatzidimitriou 1995). The solid line is a best-fit Plummer profile. At Leo II's distance, $1'$ corresponds to about 0.07 kpc. Based on mass and light profiles, we derive the M/L distribution shown in the lower panel.

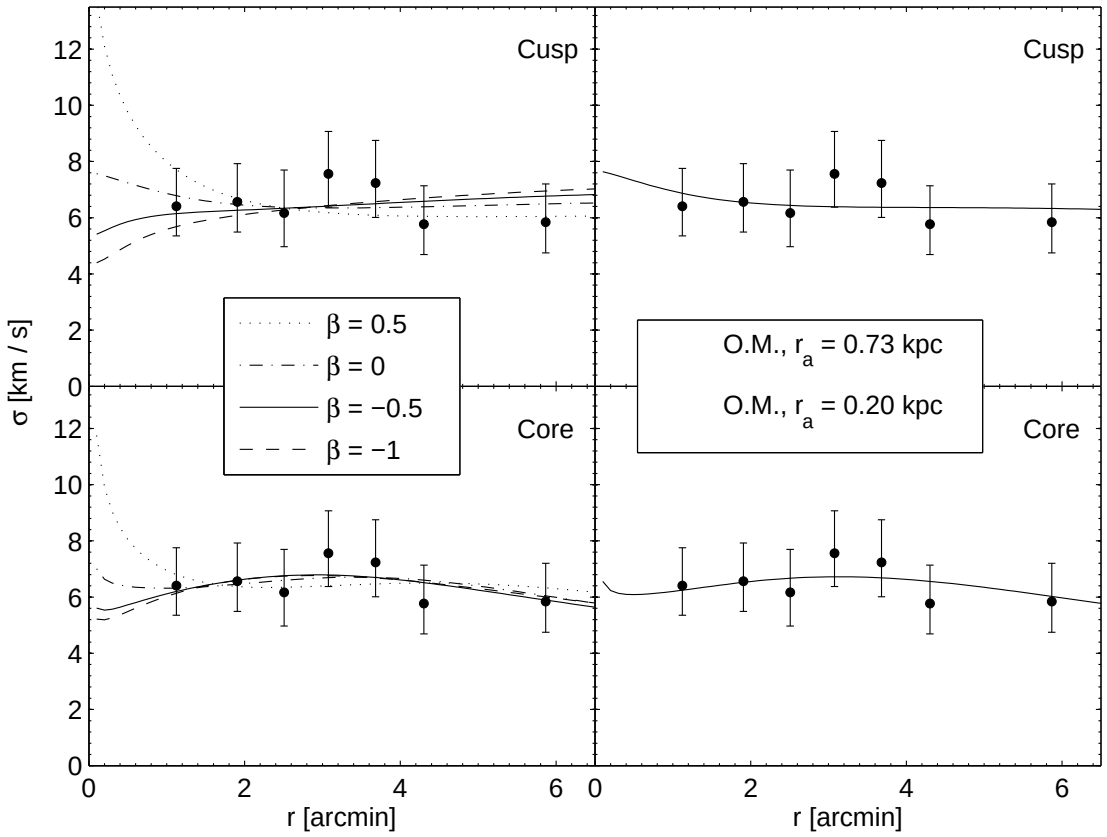

FIG. 10.— Dispersion profiles derived under the assumption of varying degrees of velocity anisotropy β. The upper and lower panels adopt two different density models, namely a NFW cusp (upper panels) and a cored halo-profile (lower panels), respectively. While the left panels maintain constant values of β, the right panels were determined for a velocity anisotropy which varies radially according to the Osipkov-Merritt (O.M.) prescription with an anisotropy radius as stated.

TABLE 1
MEASURED PROPERTIES OF RADIAL VELOCITY MEMBERS IN LEO II

Star	α (J2000)	δ (J2000)	r [$'$]	v_r	σ_{v_r}	[Fe/H]	$\sigma_{[Fe/H]}$
T_18	11 13 03.5	22 11 35.0	7.06	48.49	3.18	−1.34	0.18
T_19	11 13 23.0	22 09 23.0	1.64	78.18	5.04	−1.62	0.52
V_19	11 13 35.6	22 09 06.0	1.68	76.33	8.59	···	···
T_20	11 13 32.1	22 09 12.0	0.77	90.10	16.29	···	···
T_21	11 13 22.7	22 08 09.0	2.11	83.99	3.53	−1.75	0.25

Note. — This Table is published in its entirety in the electronic edition of the *Astronomical Journal*. A portion is shown here for guidance regarding its form and content. Metallicities are those from Paper I.